Monthly Notices
of the
ROYAL ASTRONOMICAL SOCIETY

MNRAS **462,** 1551–1562 (2016)
Advance Access publication 2016 July 20

doi:10.1093/mnras/stw1740

On the aliphatic versus aromatic content of the carriers of the 'unidentified' infrared emission features

X. J. Yang,[1,2] R. Glaser,[3] Aigen Li[2]★ and J. X. Zhong[1]

[1]*Department of Physics, Xiangtan University, 411105 Xiangtan, Hunan Province, China*
[2]*Department of Physics and Astronomy, University of Missouri, Columbia, MO 65211, USA*
[3]*Department of Chemistry, University of Missouri, Columbia, MO 65211, USA*

Accepted 2016 July 15. Received 2016 July 9; in original form 2015 July 4

ABSTRACT

Although it is generally accepted that the unidentified infrared emission (UIE) features at 3.3, 6.2, 7.7, 8.6, and 11.3 μm are characteristic of the stretching and bending vibrations of aromatic hydrocarbon materials, the exact nature of their carriers remains unknown: whether they are free-flying, predominantly *aromatic* gas-phase molecules, or amorphous solids with a *mixed aromatic/aliphatic* composition are being debated. Recently, the 3.3 and 3.4 μm features which are commonly respectively attributed to aromatic and aliphatic C–H stretches have been used to place an upper limit of ∼2 per cent on the aliphatic fraction of the UIE carriers (i.e. the number of C atoms in aliphatic chains to that in aromatic rings). Here we further explore the aliphatic versus aromatic content of the UIE carriers by examining the ratio of the observed intensity of the 6.2 μm aromatic C–C feature ($I_{6.2}$) to that of the 6.85 μm aliphatic C–H deformation feature ($I_{6.85}$). To derive the intrinsic oscillator strengths of the 6.2 μm stretch ($A_{6.2}$) and the 6.85 μm deformation ($A_{6.85}$), we employ density functional theory to compute the vibrational spectra of seven methylated polycyclic aromatic hydrocarbon molecules and their cations. By comparing $I_{6.85}/I_{6.2}$ with $A_{6.85}/A_{6.2}$, we derive the fraction of C atoms in methyl(ene) aliphatic form to be at most ∼10 per cent, confirming the earlier finding that the UIE emitters are predominantly aromatic. We have also computed the intrinsic strength of the 7.25 μm feature ($A_{7.25}$), another aliphatic C–H deformation band. We find that $A_{6.85}$ appreciably exceeds $A_{7.25}$. This explains why the 6.85 μm feature is more frequently detected in space than the 7.25 μm feature.

Key words: dust, extinction – ISM: lines and bands – ISM: molecules – infrared: ISM.

1 INTRODUCTION

A series of strong and relatively broad infrared (IR) emission features at 3.3, 6.2, 7.7, 8.6, and 11.3 μm are ubiquitously seen in almost all astronomical objects with associated gas and dust, including protoplanetary nebulae, planetary nebulae, reflection nebulae, young stellar objects, H II regions, the Galactic IR cirrus, and external galaxies (see Tielens 2008). These features are a common characteristic of the interstellar medium (ISM) of the Milky Way and nearby galaxies as well as distant galaxies out to redshifts of $z \gtrsim 4$ (e.g. see Riechers et al. 2014). Since their first detection four decades ago in two planetary nebulae (NGC 7027 and BD+30°3639; Gillett, Forrest & Merrill 1973), the carriers of these IR emission features have remained unidentified. Because of this, they are collectively known as the 'unidentified infrared emission' (UIE or UIR) bands. Nevertheless, it is now generally accepted that these features are characteristic of the stretching and bending vibrations of some sorts of aromatic hydrocarbon materials and, therefore, the UIE features are sometimes also referred to as the 'aromatic infrared bands' (AIB).

A large number of candidate materials have been proposed as carriers of the UIE bands. All of these materials contain aromatic structures of fused benzene rings. The major debate lies in the exact structure of the UIE carriers: (1) are they free-flying, predominantly *aromatic gas-phase* macro-molecules like polycyclic aromatic hydrocarbon (PAH) molecules (Léger & Puget 1984; Allamandola, Tielens & Barker 1985, 1989), or (2) are they amorphous *solids* with a *mixed aromatic/aliphatic* composition like hydrogenated amorphous carbon (HAC; Jones, Duley & Williams 1990), quenched carbonaceous composites (QCC; Sakata et al. 1990), coal or kerogen (Papoular et al. 1989)? As originally suggested by Duley & Williams (1981), all of these *solid* materials share the basic molecular structure of PAHs by containing arenes.[1] They also contain

[1] A benzene ring is C_6H_6. If the H atoms are gone, then it is not really 'benzene' anymore. It is an aromatic ring system which can be called 'arene'. Arene is a hydrocarbon with alternating double and single bonds between carbon atoms forming rings.

★ E-mail: lia@missouri.edu

aliphatic C–H bonds as well as other molecular structures often with other elements besides C and H. The 'MAON' model recently proposed by Kwok & Zhang (2011, 2013) also falls in this category, where MAON stands for '*mixed aromatic/aliphatic organic nanoparticle*'.

Are the UIE carriers aromatic or aliphatic? A straightforward way to address this question is to examine the *aliphatic fraction* of the UIE carriers (i.e. the fraction of C atoms in aliphatic chains). Aliphatic hydrocarbons have a vibrational band at 3.4 μm due to the C–H stretching mode (Pendleton & Allamandola 2002). In many interstellar and circumstellar environments the 3.3 μm emission feature is indeed often accompanied by a weaker feature at 3.4 μm (see Li & Draine 2012 and references therein). As demonstrated by Li & Draine (2012) and Yang et al. (2013), one can place an upper limit of ∼2 per cent on the aliphatic fraction of the emitters of the UIE features by assigning the 3.4 μm emission *exclusively* to aliphatic C–H (also see Rouillé et al. 2012; Steglich et al. 2013). This is indeed an *upper limit* as the 3.4 μm emission feature could also be due to *anharmonicity* of the aromatic C–H stretch (Barker, Allamandola & Tielens 1987) and '*superhydrogenated*' PAHs whose edges contain excess H atoms (Bernstein, Sandford & Allamandola 1996; Sandford, Bernstein & Materese 2013).

In addition to the 3.4 μm C–H stretching mode, aliphatic hydrocarbon materials also have two C–H deformation bands at 6.85 and 7.25 μm. These two bands have been observed in weak *absorption* in the Galactic diffuse ISM (Chiar et al. 2000). They are also seen in *emission*, with the 6.85 μm feature detected both in the Milky Way and in the Large and Small Magellanic Clouds while the 7.25 μm feature so far mostly seen in the Magellanic Clouds (e.g. see Sloan et al. 2014). Their strengths (relative to the nearby 6.2 and 7.7 μm C–C stretching bands) also allow an estimate of the aliphatic fraction of the UIE carrier.

In this work, we further explore the aliphatic versus aromatic content of the UIE carriers by examining the ratio of the observed intensity of the 6.2 μm aromatic C–C feature ($I_{6.2}$)[2] to that of the 6.85 μm aliphatic C–H deformation features ($I_{6.85}$). At this moment we will not apply the 7.25 μm emission feature to constrain the aliphatic fraction of the UIE carriers since this feature appears much weaker than the 6.85 μm feature.[3] Nevertheless, to help understand why the 6.85 μm feature is more frequently detected than the 7.25 μm feature, we will also compute the intrinsic strength of the 7.25 μm feature and compare it with the 6.85 μm feature. To derive the intrinsic oscillator strengths of the 6.2 μm aromatic C–C stretch ($A_{6.2}$) and the 6.85 μm aliphatic C–H deformation ($A_{6.85}$), we employ density functional theory to compute the IR vibrational spectra of seven methylated PAH molecules and their cations. The methyl group is taken to represent the aliphatic component of the UIE carriers. PAH cations with aliphatic sidegroups are of particular interest since ionized PAHs are expected to be dominant or at least as abundant as neutrals in astronomical environments in which the 6.2, 7.7, and 8.6 μm bands are observed. In Section 2 we briefly describe the computational methods and the parent molecules based on which we derive the band strengths. We also present in Section 2 the computed band-strength ratios $A_{6.85}/A_{6.2}$ and $A_{7.25}/A_{6.2}$. We summarize in Section 3 the intensities of the 6.2 μm aromatic C–C stretch and the 6.85 and 7.25 μm aliphatic C–H deformations observed in the Milky Way and Magellanic Clouds. In Section 4 we estimate the aliphatic fractions of the UIE carriers from the observed intensity ratio ($I_{6.85}/I_{6.2}$). We discuss and summarize our major results in Sections 5 and 6, respectively.

2 COMPUTING $A_{6.85}/A_{6.2}$ AND $A_{7.25}/A_{6.2}$

We use the GAUSSIAN09 software (Frisch et al. 2009) to calculate the IR vibrational spectra for a range of methylated aromatic molecules and their cations. We employ the hybrid density functional theoretical method (B3LYP) at the 6-311+G** level.[4] We adopt the vibrational frequency scale factor of ∼0.9688 for the B3LYP/6-311+G** method (Borowski 2012). We have considered both neutral and singly-ionized benzene (C_6H_6), naphthalene ($C_{10}H_8$), anthracene ($C_{14}H_{10}$), phenanthrene ($C_{14}H_{10}$), pyrene ($C_{16}H_{10}$), perylene ($C_{20}H_{12}$), and coronene ($C_{24}H_{12}$), as well as all of their methyl derivatives. We focus on methyl-substituted PAHs as PAHs with larger side chains are not as stable against photolytic dissociation as methyl-PAHs and are therefore not expected to be present in the ISM in a large abundance.

The molecules studied are shown in Fig. 1 together with the standard *International Union of Pure and Applied Chemistry* (IUPAC) numbering scheme.[5] We use the first four letters of the molecules to refer to them and attach the position number of the location of the methyl group. For example, 1-methylnaphthalene is referred to as Naph1. The methyl conformations are indicated in Fig. 1 and there are several possibilities. For their cation counterparts, we add a '+' sign (e.g. Naph1+ refers to singly ionized 1-methylnaphthalene).

Depending on the symmetry of the neutral molecule, there are one or two stereoisomers in which one of the methyl-CH bonds lies in the plane of the arene. We differentiate between these stereoisomers by addition of '*a*' or '*b*' to the name of the structure isomer, and the in-plane C–H bond points into the less (more) crowded hemisphere in the *a*-conformation (*b*-conformation).[6] In most cases, either the

[2] The 7.7 μm C–C stretching feature is often stronger than the 6.2 μm C–C stretch for most of the interstellar UIE sources. However, the IR vibrational spectra of methylated PAHs calculated from density function theory are too complicated in the 7.7 μm wavelength range to allow us to reliably identify the C–C stretching modes from which the 7.7 μm feature originates. In contrast, the C–C stretching modes in the 6.2 μm wavelength range are much 'cleaner'.

[3] The detection of the 7.25 μm emission feature has so far only been reported in several protoplanetary nebulae and one planetary nebula in the Magellanic Clouds (see Sloan et al. 2014). This feature is not seen in the Milky Way except in some protoplanetary discs around young stars (e.g. see Sloan et al. 2005; Acke et al. 2010; Seok & Li 2016).

[4] Yang et al. (2013) have carried out computations with the B3LYP method in conjunction with a variety of basis sets: 6-31G*, 6-31+G*, 6-311+G*, 6-311G**, 6-31+G**, 6-31++G**, 6-311+G**, 6-311++G**, 6-311+G(3df,3pd), and 6-311++G(3df,3pd). It is found that the results computed with the basis sets 6-311+G**, 6-311++G**, 6-311+G(3df,3pd), and 6-311++G(3df,3pd) essentially reach the convergence limit. The B3LYP/6-311+G** method presents an excellent compromise between accuracy and computational demand. Yang et al. (2013) have also examined the accuracy of the B3LYP method by employing second-order Møller–Plesset perturbation theory (MP2) which is thought to be more accurate in computing band intensities than B3LYP (see Cramer 2004). It is found that the results computed from B3LYP/6-311++G(3df,3pd) closely agree with that from MP2/6-311++G(3df,3pd). Therefore, in this work we adopt the B3LYP/6-311+G** method.

[5] http://www.iupac.org

[6] Take Naph1a and Naph1b as examples. In Naph1a, the in-plane methyl-H is four bonds away from the closest H-atom, H at C2. In Naph1b, the in-plane methyl-H is five bonds away from the closest H-atom, H at C8. This leaves more space between the in-plane methyl-H and H(C2) in Naph1a than between in-plane methyl-H and H(C8) in Naph1b, and Naph1a is less crowded than Naph1b.

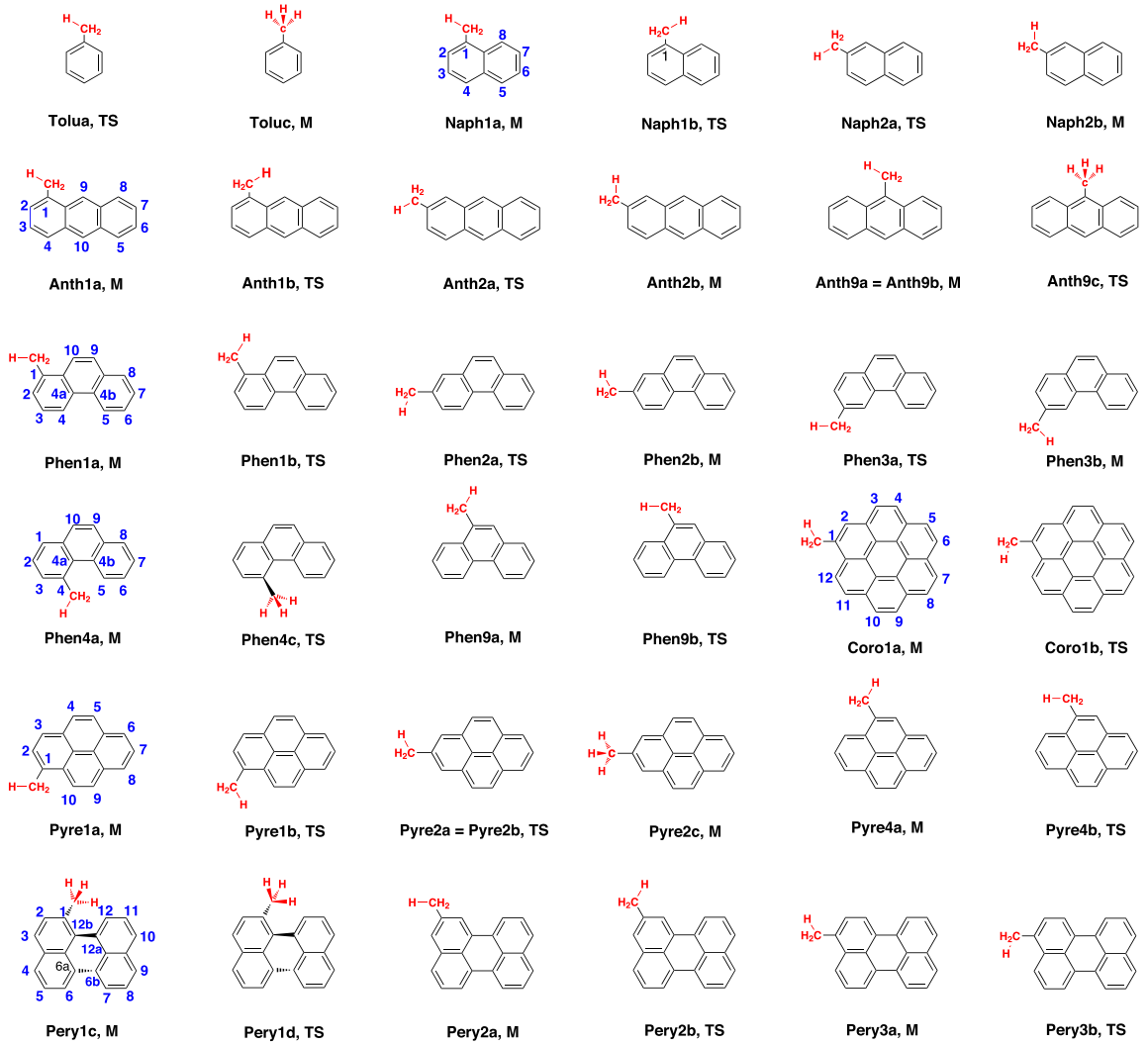

Figure 1. Structures of the mono-methyl ($-CH_3$) derivatives of seven aromatic molecules together with the standard IUPAC numbering: benzene (C_6H_6), naphthalene ($C_{10}H_8$), anthracene ($C_{14}H_{10}$), phenanthrene ($C_{14}H_{10}$), pyrene ($C_{16}H_{10}$), perylene ($C_{20}H_{12}$), and coronene ($C_{24}H_{12}$). We use the first four letters of the parent molecules to refer to them and attach the position number of the location of the methyl group (e.g. Naph1 for 1-methylnaphthalene). The mono-methyl derivative of benzene is known as toluene (i.e. 'Tolu', C_7H_8). Depending on where the methyl side-group is attached, a molecule will have several isomers (e.g. monomethyl-pyrene has three isomers in which the $-CH_3$ group is attached to carbon 1, 2, or 4, respectively). We also indicate whether the structure is a minimum (M) or a transition state (TS) structure for the methyl rotation.

a-conformation or the *b*-conformation corresponds to the minimum while the other conformation corresponds to the transition state structure for methyl rotation.[7] Note that the *a*-conformation can be the minimum (i.e. Naph1a) or the rotational transition state structure (i.e. Naph2a).

[7] A structure on the potential energy surface is a 'stationary structure' if the net inter-atomic forces on each atom are acceptably close to zero. A 'minimum' is a stationary structure for which a small distortion along any internal coordinate increases the energy (all curvatures are positive). A 'transition state structure' is a stationary structure for which a small distortion along one internal coordinate lowers the energy while distortions along any of the other internal coordinates increases the energy. The internal coordinate with the negative curvature is called the 'transition vector'. For the rotational transition state structures, the transition vector describes a rotation of the methyl group about the H_3C–C bond and serves to scramble the H atoms in the associated minimum structures (i.e. Naph1a can be realized with any one of the three methyl-Hs in the plane).

The neutral molecules Tolu, Anth9 and Pyre2 are symmetric and the *a*- and *b*-conformations are identical. In these cases there exists an additional conformation type, the *c*-conformation, in which one of the methyl-CH bonds is almost perpendicular with respect to the arene plane. For Tolu and Pery2, the *c*-conformation is the minimum while the conformations with in-plane CH-bonds are the rotational transition state structures. In contrast, for Anth9 the *c*-conformation serves as the transition state for interconversion between the conformations with in-plane CH-bonds.

We have also calculated all the minima of the cations of all the isomers of the methyl derivatives of the PAH molecules shown in Fig. 1. The structures and Mulliken charge distributions of these cations are shown in Fig. 2. The presence of a positive charge in the π-system causes polarization and results in complicated charge patterns which are characterized by positively charged centres and centres with partial negative charges. The centres of positive charges are always tertiary carbons (attached to three C atoms), while the centres of partial negative charges are secondary carbons (attached

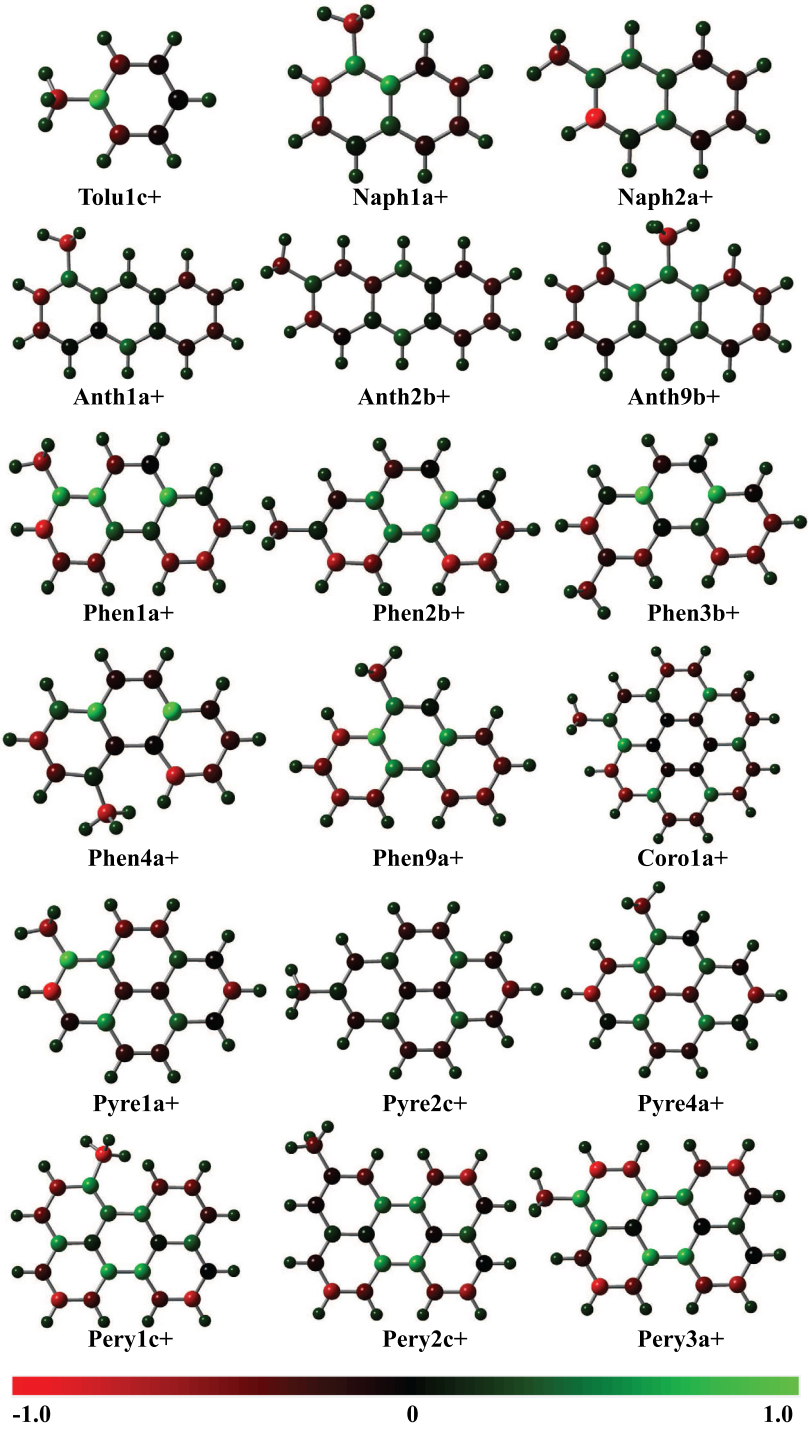

Figure 2. Charge distributions of the cations of the mono-methyl ($-CH_3$) derivatives of seven aromatic molecules: benzene, naphthalene, anthracene, phenanthrene, pyrene, perylene, and coronene. We adopt the same naming code as in Fig. 1, with a '+' sign specifying that the molecule is singly ionized. The bottom horizontal bar shows the colour coding for the charge distribution, with red being negatively charged and green being positively charged.

to two C atoms) and primary carbons (attached to one C atom). The monocyclic aromatic hydrocarbon Tolu1c+ is atypical in that it is the only cation with only one tertiary carbon and thus this carbon is the centre of positive charges. All PAHs contain tertiary carbons at the bonds shared between rings and these carbons have the capacity to accept partial positive charges. Charge delocalization is highly effective in only a few of the cations (Anth1a+, Anth2b+, Pyre2c+). Most cations prefer a distribution of charges over two or more C atoms and concomitant bond polarizations, with Pery3a+ being an extreme example.

The variety of charge distribution patterns has several consequences on the vibrational properties. First, the methyl group may be overall neutral (i.e. Pyre2c+); it may contain a partially negative methyl C (i.e. Naph1a+, Antha1a+, and especially Pery2c+); the methyl group may be attached to a cationic centre (i.e. Tolu1c+, Phen1a+) or to an essentially uncharged carbon (i.e. Anth2b+,

Table 1. IR intensity (km mol^{-1}) of the 6.85 and 7.25 μm aliphatic C–H deformation bands and the 6.2 μm aromatic C–C stretch band computed at the B3LYP/6-311+G** level for all the neutral methyl PAHs shown in Fig. 1.

Compound	$A_{6.2}$[a]	$A_{6.85}$[b]	$A_{6.85}/A_{6.2}$	$A_{7.25}$[c]	$A_{7.25}/A_{6.2}$
Toluc	1.57	6.92	4.40	0.44	0.28
Naph1a	0.81	5.25	6.53	0.58	0.71
Naph2b	1.76	4.63	2.63	0.25	0.14
Anth1a	0.68	6.83	9.97	1.32	1.93
Anth2b	1.66	7.82	4.70	0.49	0.30
Anth9a	0.41	8.66	20.98	1.61	3.89
Phen1a	0.61	9.94	16.21	1.36	2.21
Phen2b	1.27	11.04	8.68	0.08	0.06
Phen3b	1.33	8.05	6.05	0.24	0.18
Phen4a	0.40	7.84	19.39	1.00	2.47
Phen9a	0.69	4.05	5.87	2.54	3.69
Pyre1a	0.82	7.68	9.42	0.74	0.86
Pyre2c	2.37	6.28	2.65	0.19	0.08
Pyre4a	1.23	4.85	3.94	0.77	0.59
Pery1c	1.26	4.90	3.89	1.17	0.93
Pery2a	3.01	6.80	2.26	0.71	0.24
Pery3a	1.83	5.75	3.14	5.20	2.84
Coro1a	0.79	4.80	6.09	1.46	1.86

Notes. [a]Intensity of the aromatic C–C stretch at 6.2 μm in km mol^{-1} (per C–C bond).
[b]Intensity of the aliphatic C–H deformation at 6.85 μm in km mol^{-1} (per C–H bond).
[c]Intensity of the aliphatic C–H deformation at 7.25 μm in km mol^{-1} (per C–H bond).

Pyre2c+). As a result, the force constants of the aliphatic C–H modes will vary much more in the cations than in the neutral PAHs. Secondly, the charge distribution creates more diversity in the bond strengths of the aromatic C–H and of the C–C bonds and the group vibrations will cover broader spectral ranges. Thirdly, the presence of a charge and the resulted charge distribution pattern affect the dipole polarizabilities and cause significant differences in the intensities of the cations as compared to the neutrals.

The vibrational frequencies and intensities for the 6.2 μm aromatic C–C stretching mode and the 6.85 and 7.85 μm aliphatic C–H deformation modes of all the isomers of the seven methylated PAH species and their cations are computed. The standard scaling is applied to the frequencies by employing a scale factor of ∼0.9688. The scaling will not be applied to the intensities since we are mostly interested in the intensity ratios $A_{6.85}/A_{6.2}$ and $A_{7.25}/A_{6.2}$ and the scaling will be cancelled out.

We tabulate the computed band strengths in Tables 1 and 2, respectively, for neutral methyl PAHs and their cations. As shown in Fig. 3(a), both $A_{6.2}$ and $A_{6.85}$ vary appreciably for different neutral molecules and their isomers. For the 6.2 μm aromatic C–C stretch, it has an average value (per aromatic C–C bond) of $\langle A_{6.2}\rangle \approx 1.25$ km mol^{-1}, with a standard deviation of $\sigma(A_{6.2}) \approx 0.70$ km mol^{-1}. The 6.85 μm aliphatic C–H deformation band is relatively less dependent on the nature of the molecule and the specific isomer. The average band strength (per aliphatic C–H bond) is $\langle A_{6.85}\rangle \approx 6.78$ km mol^{-1}, and the standard deviation is $\sigma(A_{6.85}) \approx 1.93$ km mol^{-1}. The $A_{6.85}/A_{6.2}$ ratio, as shown in Fig. 3(b), varies considerably and depends significantly on the specific molecule and its specific isomers. Nevertheless, the $A_{6.85}/A_{6.2}$ ratio for neutral molecules clearly shows a low-end value of ∼5 (i.e. $A_{6.85}/A_{6.2} \gtrsim 5$). For these molecules, the intrinsic strength of the 7.25 μm aliphatic C–H deformation band, $A_{7.25}$, is substantially weaker than the 6.85 μm band. As shown in Fig. 4(a), the strength (per aliphatic C–H bond) of the 7.25 μm band is less than ∼2 km mol^{-1} for ∼72 per cent of the molecules and less than ∼1 km mol^{-1} for ∼61 per cent of the molecules. Similar to the 6.85 μm band, although the $A_{7.25}/A_{6.2}$ ratio varies considerably for different molecules and their different isomers, the $A_{7.25}/A_{6.2}$ ratio also clearly shows a low-end value of ∼1.0 (i.e. $A_{7.25}/A_{6.2} \gtrsim 0.5$; see Fig. 4b).

Table 2. Same as Table 1 but for the cations of all the isomers of the methyl PAHs shown in Fig. 1.

Compound	$A_{6.2}$	$A_{6.85}$	$A_{6.85}/A_{6.2}$	$A_{7.25}$	$A_{7.25}/A_{6.2}$
Toluc+	0.10	6.73	66.27	0.90	8.82
Naph1a+	0.42	12.08	28.66	9.91	23.51
Naph2a+	4.92	9.86	2.00	9.49	1.93
Anth1a+	4.25	13.70	3.22	4.95	1.17
Anth2b+	6.74	8.96	1.33	0.76	0.11
Anth9b+	7.24	6.40	0.88	9.66	1.33
Phen1a+	10.90	13.17	1.21	4.71	0.43
Phen2b+	14.56	6.04	0.42	0.82	0.06
Phen3b+	23.22	9.37	0.40	6.97	0.30
Phen4a+	10.92	9.68	0.89	6.46	0.59
Phen9a+	11.24	4.98	0.44	6.73	0.60
Pyre1a+	12.70	10.07	0.79	0.93	0.07
Pyre2c+	9.59	6.15	0.64	1.39	0.14
Pyre4a+	12.83	6.84	0.53	1.50	0.12
Pery1c+	9.32	8.81	0.95	2.43	0.26
Pery2c+	3.21	4.19	1.30	1.64	0.51
Pery3a+	10.74	7.24	0.67	0.98	0.09
Coro1a+	16.98	18.47	1.09	2.83	0.17

For the cations of the methyl PAHs considered in this work, the computed band strengths ($A_{6.85}$, $A_{7.25}$) and their ratios ($A_{6.85}/A_{6.2}$, $A_{7.25}/A_{6.2}$) are tabulated in Table 2 and shown in Fig. 5. Compared to their neutral counterparts, the band-strength ratios of cations show even more substantial differences among different molecules. However, similar to neutral molecules, the band-strength ratios of cations also show low-end values, with $A_{6.85}/A_{6.2} \gtrsim 0.5$ and $A_{7.25}/A_{6.2} \gtrsim 0.25$, respectively, for the 6.85 and 7.25 μm bands.

3 OBSERVATIONAL CONSTRAINTS

Unlike the 3.4 μm aliphatic C–H stretch, the detection of the 6.85 and 7.25 μm aliphatic C–H deformation bands in the ISM of the Milky Way is much rarer. We are not aware of any Galactic sources in which the 7.25 μm feature is seen in emission except several protoplanetary discs (Seok & Li 2016). On the other hand, to the best of our knowledge, only seven *Galactic* objects exhibit a noticeable emission feature at 6.85 μm: NGC 7023, a reflection nebula (RN); NGC 7027, a planetary nebula (PN), the Orion bar, a photodissociated region (PDR); and four protoplanetary nebulae (PPNe; IRAS 01005+7910, IRAS 04296+3429, IRAS 22223+4327, and IRAS 22272+5435). Except for the four Galactic PPNe, the observed 6.85 μm feature intensity is much weaker than that of the 6.2 μm feature. As shown in Table 3, for Galactic sources other than PPNe, $I_{6.85}/I_{6.2} \lesssim 0.10$. For the four Galactic PPNe, the 6.85 μm feature is much stronger, with $I_{6.85}/I_{6.2} > 1$ for three of these four PPNe. However, these Galactic PPNe all exhibit 'unusual' UIE properties compared to the typical interstellar UIE bands (e.g. these PPNe show a broad 8.2 μm feature rather than separately resolved 7.7/8.6 μm UIE features; moreover, the 11.3 and 12.7 μm C–H out-of-plane bending features seen in sources with 'normal'-looking UIE features are blended in a flat-top broad-band at ∼11.8 μm; see

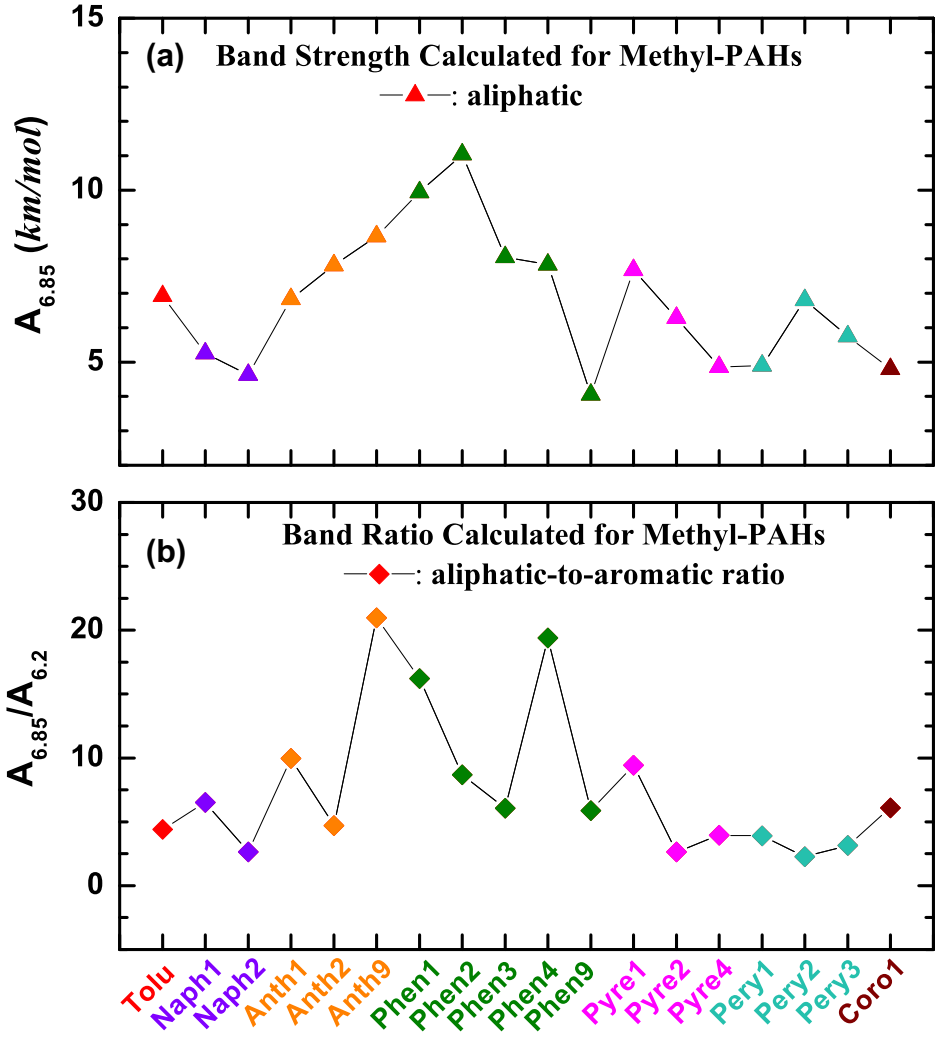

Figure 3. Band strengths for the 6.85 μm aliphatic C–H deformation ($A_{6.85}$) and for the ratio of $A_{6.85}$ to the 6.2 μm aromatic C–C stretch ($A_{6.2}$) as determined with the B3LYP/6-311+G** method for the mono-methyl derivatives of seven aromatic neutral molecules (benzene, naphthalene, anthracene, phenanthrene, pyrene, perylene, and coronene) and all of their isomers.

Tokunaga 1997, Peeters et al. 2002). The origin of these 'unusual' UIE features is unclear and their carriers are very likely different from that of the normal-looking interstellar UIE features. While the UIE carriers of PPNe are freshly synthesized in the outflows of asymptotic giant branch (AGB) and/or post-AGB stars, their interstellar counterparts must have experienced various physical and chemical processes in the ISM. In this work we will restrict ourselves to the interstellar sources which show typical-looking UIE features for which $I_{6.85}/I_{6.2} \lesssim 0.10$.

It is interesting to note that the 6.85 and 7.25 μm emission features appear to be more frequently seen in the Magellanic Clouds than in the Galaxy. Sloan et al. (2014) systematically analysed the *Spitzer*/IRS spectra of a large number of carbon-rich sources in the Large and Small Magellanic Clouds. They derived the intensities of the 6.2, 6.85, 7.25, 7.7 and 8.6 μm emission features of all the Magellanic sources which exhibit the 6.85 and 7.25 μm emission features. We compile the observed intensity ratios $I_{6.85}/I_{6.2}$ and $I_{7.25}/I_{6.2}$ from Sloan et al. (2014) for all these sources and tabulate them in Table 3 and show them in Fig. 6. These sources are predominantly PPNe, with only three out of 18 not PPNe: SMP SMC 011 (PN), SMP SMC 020 (PN), and IRAS 05360−7121 (AGB). While the Magellanic PPNe have a wide range of intensity ratios from $I_{6.85}/I_{6.2} \lesssim 0.1$ to $I_{6.85}/I_{6.2} \gtrsim 1.0$ and from $I_{7.25}/I_{6.2} \lesssim 0.05$ to $I_{7.25}/I_{6.2} \gtrsim 0.2$, two of the non-PPN sources (SMP SMC 011, IRAS 05360−7121) have $I_{6.85}/I_{6.2} \lesssim 0.06$ and one non-PPN source (SMP SMC 020) has $I_{6.85}/I_{6.2} \sim 0.2$. The 7.25 μm feature is not seen in SMP SMC 011 and IRAS 05360−7121. Even in SMP SMC 020, the only non-PPN source in the Magellanic Clouds in which the detection of the 7.25 μm feature was reported, the intensity ratio has a large error bar (i.e. $I_{7.25}/I_{6.2} \approx 0.14 \pm 0.11$). Combining the intensity ratios observed for both Galactic and Magellanic sources, in the following we will take $I_{6.85}/I_{6.2} = 0.1$ to determine the aliphatic fractions of the UIE carriers. The 7.25 μm emission feature will not be used to estimate the aliphatic content of the UIE carriers.

4 CONSTRAINTS ON THE ALIPHATIC FRACTION OF THE UIE CARRIERS FROM THE 6.85 μm FEATURES

Let $N_{\rm C,\,ali}$ and $N_{\rm C,\,aro}$, respectively, be the numbers of aliphatic and aromatic C atoms in the emitters of the 6–8 μm UIE bands. Let $B_\lambda(T) = (2hc^2/\lambda^5)/[\exp(hc/\lambda kT) - 1]$ be the *Planck* function at

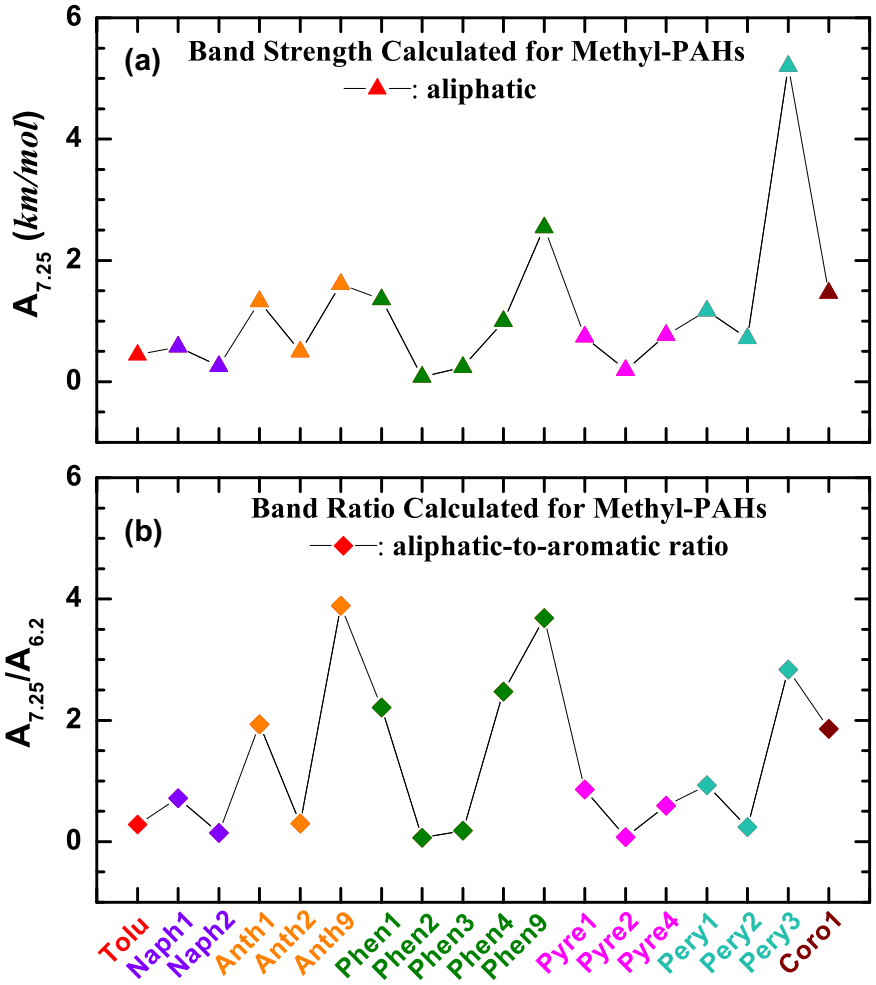

Figure 4. Same as Fig. 3 but for the 7.25 μm aliphatic C–H deformation band ($A_{7.25}$).

wavelength λ and temperature T (where h is the *Planck* constant, c is the speed of light, and k is the Boltzman constant). The aliphatic fraction can be estimated from

$$\frac{N_{\rm C,ali}}{N_{\rm C,aro}} \approx \frac{I_{6.85}}{I_{6.2}} \times \frac{A_{6.2}}{A_{6.85}} \times \frac{B_{6.2}}{B_{6.85}} \times \left(\frac{1.25}{2.5}\right), \quad (1)$$

where the term (1.25/2.5) arises from that we assume that one aliphatic C atom corresponds to 2.5 aliphatic C–H bonds (intermediate between methylene $-CH_2$ and methyl $-CH_3$) and one aromatic C atom corresponds to 1.25 aromatic C–C bond (intermediate between benzene C_6H_6 and coronene $C_{24}H_{12}$). The major UIE features fall in the wavelength range of ∼3–12 μm, implying a temperature range of $200 \lesssim T \lesssim 800$ K.[8] With $I_{6.85}/I_{6.2} \lesssim 0.10$ and $B_{6.85}/B_{6.2} \approx 1.04 \pm 0.24$ for $200 \lesssim T \lesssim 800$ K we obtain an upper limit of $N_{\rm C,\,ali}/N_{\rm C,\,aro} \approx 0.96$ per cent for neutral methylated-PAHs with $A_{6.2}/A_{6.85} \lesssim 0.2$, and $N_{\rm C,\,ali}/N_{\rm C,\,aro} \approx 9.6$ per cent for ionized methylated-PAHs with $A_{6.2}/A_{6.85} \lesssim 2.0$. We therefore conclude that the carriers of the 6–8 μm UIE bands are largely aromatic, with <10 per cent of the C atoms in aliphatic form.

[8] Let $C_{\rm abs}(\lambda)$ be the dust absorption cross-section at wavelength λ and j_λ be the dust IR emissivity. For $C_{\rm abs}(\lambda) \propto \lambda^{-\beta}$, λj_λ peaks at $\lambda_p \approx (hc/kT)/(4+\beta)$ (see Li 2005). With $\beta \approx 2$ for PAH-like UIE carriers, we have $T \approx 800$ K for $\lambda_p \sim 3$ μm and $T \approx 200$ K for $\lambda_p \sim 12$ μm.

The above derivation of $N_{\rm C,\,ali}/N_{\rm C,\,aro}$ is based on the assumption that the UIE carriers emit at a single temperature in the range of $200 \lesssim T \lesssim 800$ K. However, the UIE carriers are nano-sized (or smaller) and will be transiently heated by single stellar photons (see Li 2004). Illuminated by starlight, they will not attain an equilibrium temperature, instead, they will have a distribution of temperatures. Following Draine & Li (2001), we will calculate the temperature probability distribution functions and emission spectra of methyl PAHs of $N_{\rm C,\,aro}$ aromatic C atoms and $N_{\rm C,\,ali}$ aliphatic C atoms. For such molecules, we approximate their absorption cross-sections by adding three Drude functions to that of PAHs of $N_{\rm C,\,aro}$ C atoms. These Drude functions represent the 3.4 μm aliphatic C–H stretch, and the 6.85 and 7.25 μm aliphatic C–H deformations. The absorption cross-section of a methyl PAH molecule of $N_{\rm C,\,aro}$ aromatic C atoms and $N_{\rm C,\,ali}$ aliphatic C atoms becomes

$$C_{\rm abs}(N_{\rm C},\lambda) = C_{\rm abs}^{\rm PAH}(N_{\rm C,aro},\lambda) \quad (2)$$

$$+ N_{\rm C,ali}\frac{2}{\pi}\frac{\gamma_{3.4}\lambda_{3.4}\sigma_{\rm int,3.3}\,(A_{3.4}/A_{3.3})}{(\lambda/\lambda_{3.4}-\lambda_{3.4}/\lambda)^2+\gamma_{3.4}^2} \quad (3)$$

$$+ N_{\rm C,ali}\frac{2}{\pi}\frac{\gamma_{6.85}\lambda_{6.85}\sigma_{\rm int,6.2}\,(A_{6.85}/A_{6.2})}{(\lambda/\lambda_{6.85}-\lambda_{6.85}/\lambda)^2+\gamma_{6.85}^2} \quad (4)$$

$$+ N_{\rm C,ali}\frac{2}{\pi}\frac{\gamma_{7.25}\lambda_{7.25}\sigma_{\rm int,6.2}\,(A_{7.25}/A_{6.2})}{(\lambda/\lambda_{7.25}-\lambda_{7.25}/\lambda)^2+\gamma_{7.25}^2}, \quad (5)$$

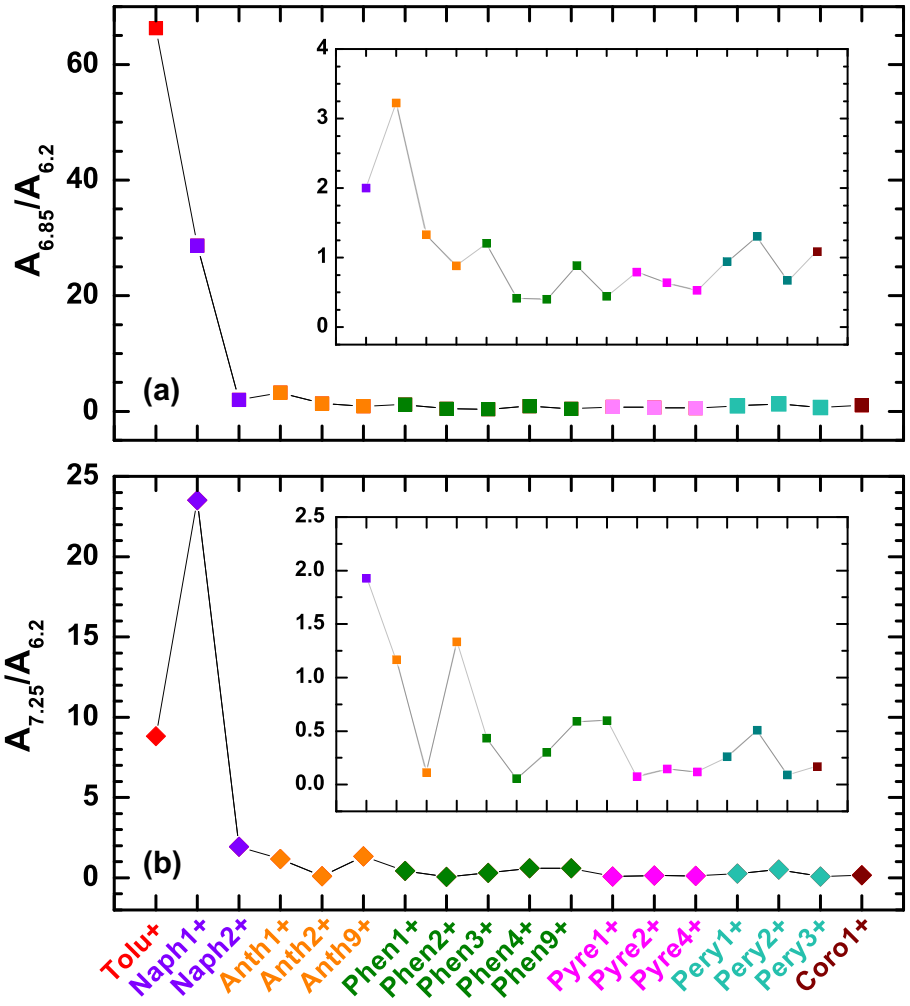

Figure 5. Band-strength ratios of the 6.85 and 7.25 μm aliphatic C–H deformation bands to the 6.2 μm aromatic C–C stretch as determined with the B3LYP/6-311+G** method for the mono-methyl derivatives of seven aromatic cations (benzene, naphthalene, anthracene, phenanthrene, pyrene, perylene, and coronene) and all of their isomers. The inset panels enlarge the band-strength ratios of those molecules with $A_{6.85}/A_{6.2} < 4$ (upper panel) and with $A_{7.25}/A_{6.2} < 2$ (bottom panel).

where $N_{\rm C} = N_{\rm C,\,aro} + N_{\rm C,\,ali}$; $\lambda_{3.4} = 3.4\,\mu$m, $\lambda_{6.85} = 6.85\,\mu$m, and $\lambda_{7.25} = 7.25\,\mu$m are, respectively, the peak wavelengths of the 3.4, 6.85 and 7.25 μm features; $\gamma_{3.4}\lambda_{3.4}$, $\gamma_{6.85}\lambda_{6.85}$, and $\gamma_{7.25}\lambda_{7.25}$ are, respectively, the full width at half-maximum of the 3.4, 6.85 and 7.25 μm features ($\gamma_{3.4}$, $\gamma_{6.85}$, and $\gamma_{7.25}$ are dimentionless parameters; see Draine & Li 2007); and $\sigma_{\rm int,\,3.3}$ and $\sigma_{\rm int,\,6.2}$ are, respectively, the integrated strengths per (aromatic) C atom of the 3.3 μm aromatic C–H stretch and 6.2 μm aromatic C–C stretch (see Draine & Li 2007). We take $A_{3.4}/A_{3.3} = 1.76$ (see Yang et al. 2013). We take the lower limits of $A_{6.85}/A_{6.2} \approx 5.0$ and $A_{7.25}/A_{6.2} \approx 0.5$ for neutrals, $A_{6.85}/A_{6.2} \approx 0.5$ and $A_{7.25}/A_{6.2} \approx 0.25$ for cations as derived in Section 2. We note that, for a given observed intensity ratio $I_{6.85}/I_{6.2}$, a lower limit on $A_{6.85}/A_{6.2}$ leads to an upper limit on the aliphatic fraction $N_{\rm C,\,ali}/N_{\rm C,\,aro}$.

Let dP be the probability that the temperature of the methyl molecule will be in $[T,\ T + dT]$. The emissivity of this molecule becomes

$$j_\lambda(N_{\rm C}) = \int C_{\rm abs}(N_{\rm C}, \lambda)\, 4\pi\, B_\lambda(T)\, \frac{dP}{dT}\, dT. \qquad (6)$$

As shown in figs 6 and 7 of Draine & Li (2007), the 6–8 μm interstellar UIE emitters are in the size range of $N_{\rm C} \sim$50–100 C atoms. For illustrative purpose, we therefore consider $N_{\rm C} = 80$. We adopt the 'thermal-discrete' method of Draine & Li (2007) to compute the temperature probability distribution functions of both neutral and ionized methyl PAHs of $N_{\rm C,\,ali} = 0, 1, 2, ..., 8$ aliphatic C atoms and $(80 - N_{\rm C,\,ali})$ aromatic C atoms. In Fig. 7 we show the IR emission spectra of both neutral and ionized methyl PAHs of $N_{\rm C,\,ali} = 0, 1, 3, 5, 8$ illuminated by the solar neighbourhood interstellar radiation field (ISRF) of Mathis, Mezger & Panagia (1983, hereafter MMP83). Fig. 7 shows that, while the 6.85 μm feature is clearly visible in the IR emission spectrum for $N_{\rm C,\,ali} = 3$, the 7.25 μm feature remains hardly noticeable even for $N_{\rm C,\,ali} = 8$. We will discuss this in more detail in Section 5. For a given $N_{\rm C,\,ali}$, we derive $(I_{6.85}/I_{6.2})_{\rm mod}$, the model intensity ratio of the 6.85 μm band to the 6.2 μm band, from

$$\left(\frac{I_{6.85}}{I_{6.2}}\right)_{\rm mod} = \frac{\int_{6.85} \Delta j_\lambda(N_{\rm C})\, d\lambda}{\int_{6.2} \Delta j_\lambda(N_{\rm C})\, d\lambda}, \qquad (7)$$

where $\int_{6.2} \Delta j_\lambda(N_{\rm C})\, d\lambda$ and $\int_{6.85} \Delta j_\lambda(N_{\rm C})\, d\lambda$ are, respectively, the feature-integrated excess emission of the methyl PAH above the 6.2 and 6.85 μm features. In Fig. 8 we show the model intensity ratios $(I_{6.85}/I_{6.2})_{\rm mod}$ as a function of $N_{\rm C,\,ali}/N_{\rm C,\,aro}$. For an observational upper limit of $(I_{6.85}/I_{6.2})_{\rm obs} \lesssim 0.1$, Fig. 8 allows us to place an upper limit of $N_{\rm C,\,ali}/N_{\rm C,\,aro} \approx 1.8$ per cent for neutral methyl PAHs and

Table 3. Observed intensity ratios of the 6.85 and 7.25 μm aliphatic C–H deformation bands to the 6.2 μm aromatic C–C stretch band ($I_{6.85}/I_{6.2}$, $I_{7.25}/I_{6.2}$).

Object	Type	$I_{6.85}/I_{6.2}$	$I_{7.25}/I_{6.2}$	Reference
NGC 7023	RN	0.043	...	This work
NGC 7027	PN	0.092	...	Kwok & Zhang (2011)
Orion Bar	PDR	0.097	...	Kwok & Zhang (2011)
IRAS 01005+7910	PPN	0.19	...	Zhang, Kwok & Hrivnak (2010)
IRAS 04296+3429	PPN	1.30	...	Zhang et al. (2010)
IRAS 22223+4327	PPN	1.86	...	Zhang et al. (2010)
IRAS 22272+5435	PPN	4.23	...	Tokunaga (1997)
IRAS 00350−7436	PPN	-0.72 ± 0.13	0.47 ± 0.24	Sloan et al. (2014)
IRAS 05063−6908	PPN	0.35 ± 0.09	0.03 ± 0.04	Sloan et al. (2014)
IRAS 05073−6752	PPN	1.05 ± 0.15	0.00 ± 0.04	Sloan et al. (2014)
IRAS 05092−7121	PPN	0.09 ± 0.01	-0.02 ± 0.01	Sloan et al. (2014)
IRAS 05110−6616	PPN	1.66 ± 0.06	0.34 ± 0.02	Sloan et al. (2014)
IRAS 05185−6806	PPN	0.06 ± 0.01	-0.02 ± 0.01	Sloan et al. (2014)
IRAS F05192−7008	PPN	0.23 ± 0.10	0.04 ± 0.09	Sloan et al. (2014)
IRAS Z05259−7052	PPN	0.33 ± 0.06	0.05 ± 0.01	Sloan et al. (2014)
IRAS 05360−7121	AGB	0.05 ± 0.01	-0.02 ± 0.01	Sloan et al. (2014)
IRAS 05413−6934	PPN	0.27 ± 0.17	-0.10 ± 0.10	Sloan et al. (2014)
IRAS 05588−6944	PPN	0.14 ± 0.02	-0.06 ± 0.02	Sloan et al. (2014)
IRAS 06111−7023	PPN	1.05 ± 0.06	0.14 ± 0.01	Sloan et al. (2014)
2MASS J00444111−7321361	PPN	1.03 ± 0.05	0.19 ± 0.02	Sloan et al. (2014)
2MASS J01054645−7147053	PPN	0.09 ± 0.02	0.00 ± 0.03	Sloan et al. (2014)
2MASS J05204385−6923403	PPN	0.42 ± 0.05	0.09 ± 0.03	Sloan et al. (2014)
NGC 1978 WBT 2665	PPN	1.69 ± 0.32	0.28 ± 0.08	Sloan et al. (2014)
SMP SMC 011	PN	0.06 ± 0.01	-0.09 ± 0.02	Sloan et al. (2014)
SMP SMC 020	PN	0.20 ± 0.08	0.14 ± 0.11	Sloan et al. (2014)

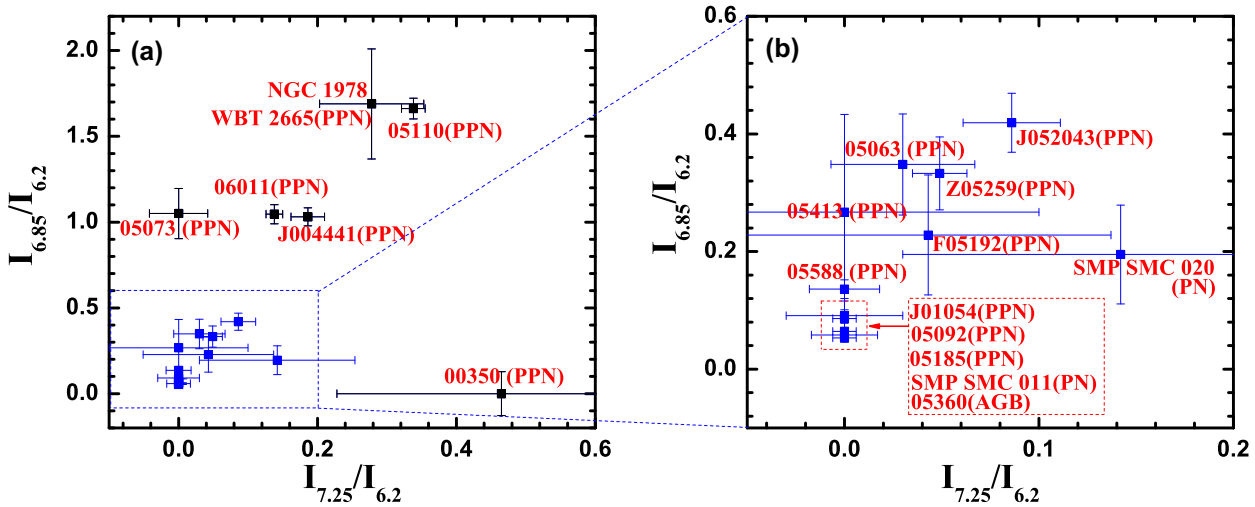

Figure 6. Observed intensity ratios $I_{6.85}/I_{6.2}$ versus $I_{7.25}/I_{6.2}$ of the Magellanic Cloud sources compiled in Sloan et al. (2014). The right panel (b) enlarges those sources shown in the left panel (a) with $I_{6.85}/I_{6.2} < 0.5$ and $I_{7.25}/I_{6.2} < 0.2$.

$N_{\rm C,\,ali}/N_{\rm C,\,aro} \approx 7.5$ per cent for ionized methyl PAHs. We therefore can also conclude that the carriers of the 6–8 μm UIE bands are largely aromatic, with < 10 per cent of the C atoms in aliphatic form.

5 DISCUSSION

In Section 4 we have shown that the aliphatic fractions derived from the simple single-temperature approach ($N_{\rm C,\,ali}/N_{\rm C,\,aro} \approx 0.96$ per cent for neutrals and $N_{\rm C,\,ali}/N_{\rm C,\,aro} \approx 9.6$ per cent for cations) are generally consistent with that derived from the more rigorous calculations of the model emission spectra ($N_{\rm C,\,ali}/N_{\rm C,\,aro} \approx$ 1.8 per cent for neutrals and $N_{\rm C,\,ali}/N_{\rm C,\,aro} \approx 7.5$ per cent for cations). This can be understood in terms of the single-photon heating process. Upon absorption of a photon of energy $h\nu$ (where ν is the photon frequency), a methyl PAH molecule will be heated to a maximum temperature T_p determined by its specific heat $C(T)$ and $h\nu$: $\int_0^{T_p} C(T)\,dT = h\nu$. The molecule will then rapidly cool down and radiate away most of the absorbed energy at temperature T_p. Before it absorbs another photon, the molecule will spend most of the time at very low temperatures (Draine & Li 2001). Therefore, a single temperature of T_p provides a reasonably good measure of the IR emission.

The aliphatic fractions derived in Section 4 from the model intensity ratio $(I_{6.85}/I_{6.2})_{\rm mod}$ are calculated for methyl PAHs excited by the MMP83 ISRF. If the actual radiation intensity is U-times that of

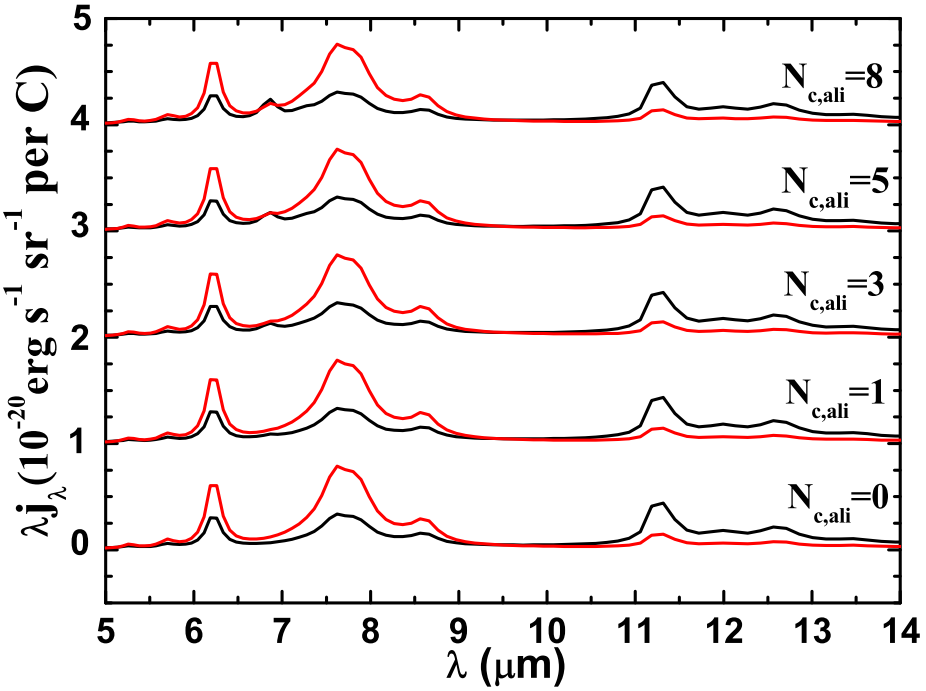

Figure 7. IR emission spectra of neutral (black lines) and ionized (red lines) methyl PAHs of $N_{\rm C,\,ali} = 0$, 1, 3, 5, 8 aliphatic C atoms and $(80 - N_{\rm C,\,ali})$ aromatic C atoms illuminated by the MMP83 ISRF. For clarity, the spectra for methyl PAHs with $N_{\rm C,\,ali} = 1$, 3, 5, 8 are vertically shifted.

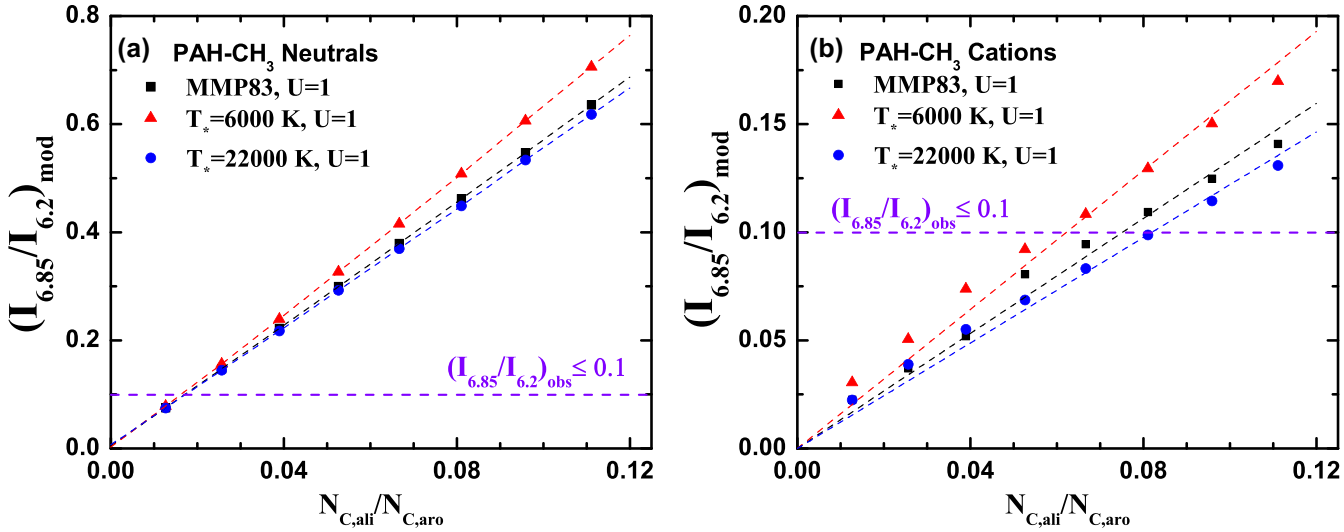

Figure 8. Model-calculated intensity ratios $(I_{6.85}/I_{6.2})_{\rm mod}$ as a function of the aliphatic fraction $N_{\rm C,\,ali}/N_{\rm C,\,aro}$ for (a) neutral methyl PAHs and (b) their cations. The molecules and their cations are illuminated by the MMP83 ISRF (squares), a solar-type star of $T_{\rm eff} = 6000$ K (triangles), and a B1.5V star of $T_{\rm eff} = 22\,000$ K (circles). The dashed horizontal line plots the observed upper limit of the intensity ratio $(I_{6.85}/I_{6.2})_{\rm obs} \lesssim 0.1$. The lines passing through the origin are linear fits to the model-calculated intensity-ratio data points.

the MMP83 ISRF, the results will remain unchanged because the IR emission spectra of stochastically heated nano-sized grains or very large molecules, after scaled by U, are essentially independent of U (e.g. see fig. 13 of Li & Draine 2001, and fig. 1(f) of Draine & Li 2007). To examine whether and how the 'hardness' of the exciting starlight affects the aliphatic fraction estimate, we consider methyl PAHs of $N_{\rm C,\,ali} = 0$, 1, 2, ..., 8 aliphatic C atoms and $(80 - N_{\rm C,\,ali})$ aromatic C atoms excited by stars with an effective temperature of $T_{\rm eff} = 6000$ K like our Sun and by stars of $T_{\rm eff} = 22\,000$ K like the B1.5V star HD 37903 which illuminates the reflection nebula NGC 2023. The starlight intensity in the 912 Å–1 μm wavelength range is fixed at $U = 1$, with U defined as

$$U \equiv \frac{\int_{1\,\mu{\rm m}}^{912\,{\rm \AA}} 4\pi\, J_\star(\lambda,\, T_{\rm eff})\, d\lambda}{\int_{1\,\mu{\rm m}}^{912\,{\rm \AA}} 4\pi\, J_{\rm ISRF}(\lambda)\, d\lambda}, \qquad (8)$$

where $J_\star(\lambda,\, T_{\rm eff})$ is the intensity of starlight approximated by the Kurucz model atmospheric spectrum, and $J_{\rm ISRF}(\lambda)$ is the MMP83 ISRF starlight intensity. As shown in Fig. 8, for a given $N_{\rm C,\,ali}/N_{\rm C,\,aro}$, the $T_{\rm eff} = 6000$ K model results in a larger $(I_{6.85}/I_{6.2})_{\rm mod}$ than that of the MMP83 ISRF model, while the $T_{\rm eff} = 22\,000$ K model results in a smaller $(I_{6.85}/I_{6.2})_{\rm mod}$ than that of the MMP83 ISRF

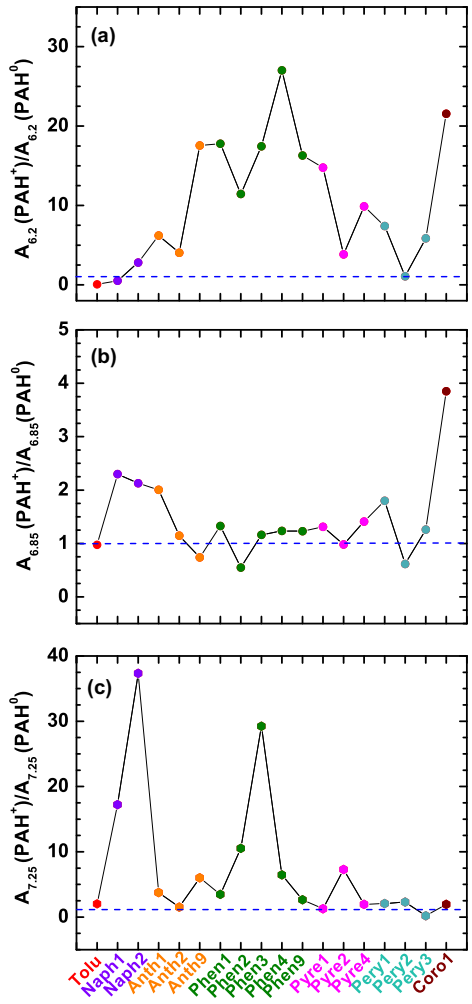

Figure 9. Effects of ionization on the intrinsic strengths of the 6.2, 6.85 and 7.25 μm bands.

model. This is because a *softer* radiation field rises the methyl PAH molecule to a *lower* temperature and therefore it radiates relatively more at 6.82 μm than at 6.2 μm. Nevertheless, the effects on the derived $N_{\rm C,\,ali}/N_{\rm C,\,aro}$ are small: the MMP83 ISRF model, the $T_{\rm eff} = 6000$ K model, and the $T_{\rm eff} = 22\,000$ K model, respectively, derive $N_{\rm C,\,ali}/N_{\rm C,\,aro} \approx 1.6$ per cent, 1.8 per cent, 1.8 per cent for neutrals, and $N_{\rm C,\,ali}/N_{\rm C,\,aro} \approx 6.2$ per cent, 7.5 per cent, 8.2 per cent for cations (see Fig. 8).

To examine the effects of ionization of methyl PAHs on the intrinsic strengths of the 6.2, 6.85 and 7.25 μm bands, we show in Fig. 9 the intrinsic strengths of these bands of ionized methyl PAHs relative to that of their neutral counterparts. As is long known (Allamandola, Hudgins & Sandford 1999; Hudgins & Allamandola 2005), the 6.2 μm C–C stretch is substantially enhanced upon ionization (see Fig. 9a). In contrast, the 6.85 μm aliphatic C–H deformation is only moderately enhanced (see Fig. 9b), while the 7.25 μm aliphatic C–H deformation is more like the 6.2 μm C–C stretch and shows considerable enhancement upon ionization (see Fig. 9c).

As mentioned in Sections 3 and 4, the detection of the 7.25 μm emission feature in the Milky Way or the Magellanic Clouds is rarer than the 6.85 μm feature. This is because, as shown in Fig. 10, the intrinsic strength of the 7.25 μm feature is weaker than that of the 6.85 μm feature by a factor of ∼8 for neutral methyl PAHs and by a factor of ∼3 for their cations. In addition, the weak 7.25 μm feature could be hidden by the pronounced 7.7 μm C–C stretch.

The aliphatic fraction of the UIE carriers derived from the 6.85 μm aliphatic C–H deformation is consistent with that derived from the 3.4 μm aliphatic C–H stretch in the sense that the UIE carrier is predominantly aromatic and the aliphatic component is only a minor part of the UIE emitters. Based on the observed intensity ratios of the 3.4 μm feature to the 3.3 μm feature, Li & Draine (2012) placed an upper limit of ∼9 per cent on the aliphatic fraction of the UIE carriers in NGC 7027 and the Orion bar. Yang et al. (2013) further constrained the aliphatic fraction to be at most ∼2 per cent by examining a large sample of 35 UIE sources which exhibit both the 3.3 μm and 3.4 μm C–H features. Unlike Li & Draine (2012) who adopted the 3.3 μm feature strength ($A_{3.3}$) of small neutral PAHs (Draine & Li 2007) and the 3.4 μm feature strength ($A_{3.4}$) obtained by averaging over three pure aliphatic molecules (i.e. ethane, hexane, and methyl-cyclo-hexane) and one aromatic molecule with an aliphatic sidegroup (i.e. ethyl-benzene; d'Hendecourt & Allamandola 1986), Yang et al. (2013) employed density functional theory to compute $A_{3.4}/A_{3.3}$ for a range of methyl-substituted PAHs.

Li & Draine (2012) have also examined the 6.85 and 7.7 μm features of NGC 7027 and the Orion bar by comparing the observed intensity ratios of these two bands ($I_{6.85}/I_{7.7}$) with their intrinsic band strengths ($A_{6.85}$, $A_{7.7}$). Adopting the 7.7 μm feature strength of charged aromatic molecules (Draine & Li 2007) for $A_{7.7}$ and the 6.85 μm feature strength obtained by averaging over that measured for methyl-cylco-hexane (d'Hendecourt & Allamandola 1986) and for HAC (Dartois & Muñoz-Caro 2007) for $A_{6.85}$, they derived the aliphatic fraction of the UIE emitters to be <15 per cent. With the band-strength ratio $A_{6.85}/A_{6.2}$ obtained over many methylated aromatic species (see Section 2), we derive an aliphatic fraction of <10 per cent from the observed intensity ratio $I_{6.85}/I_{6.2}$ (see Section 4).

Finally, we note that the aliphatic C atoms considered here are all in the form of methyl side groups. The aliphatic fraction derived in Section 4 is the ratio between the number of C atoms in the aromatic skeleton of PAHs and the number of C atoms in methyl side groups. This is not necessarily *all* of the aliphatic C atoms in astronomical PAHs: there may be some in linear bridges, and there may also be some that are in the regular PAH skeleton but at a superhydrogenated site.[9] These aliphatic C atoms are not yet included in this study. But Yang et al. (2016) have shown that the aliphatic fraction of the UIE carriers derived from the $A_{3.4}/A_{3.3}$ ratios of PAHs with a wide range of sidegroups (e.g. ethyl, propyl, butyl, dimethyl) was close to that based on the $A_{3.4}/A_{3.3}$ ratios of mono-methyl PAHs. Also, the sample of regular and methylated PAHs considered here (see Fig. 1) may not be representative of what are actually present in astronomical environments (e.g. the actual astro-PAH molecules may have $N_{\rm C} \gtrsim 40$ C atoms (Tielens 2008) while the largest molecule considered here is coronene of $N_{\rm C} = 24$). Future experimental and/or quantum-chemical computational studies of larger species would be very helpful to obtain more reliable estimates of the $A_{6.85}/A_{6.2}$ ratio, and, therefore, of the aliphatic fraction of the UIE carriers.

6 SUMMARY

We have examined the nature of the UIE emitters by comparing the observed intensity ratios of the 6.2 μm aromatic C–C stretch and the

[9] To bond to an additional H atom, a C atom has to switch from sp^2 to sp^3 orbitals, thereby by definition becoming aliphatic.

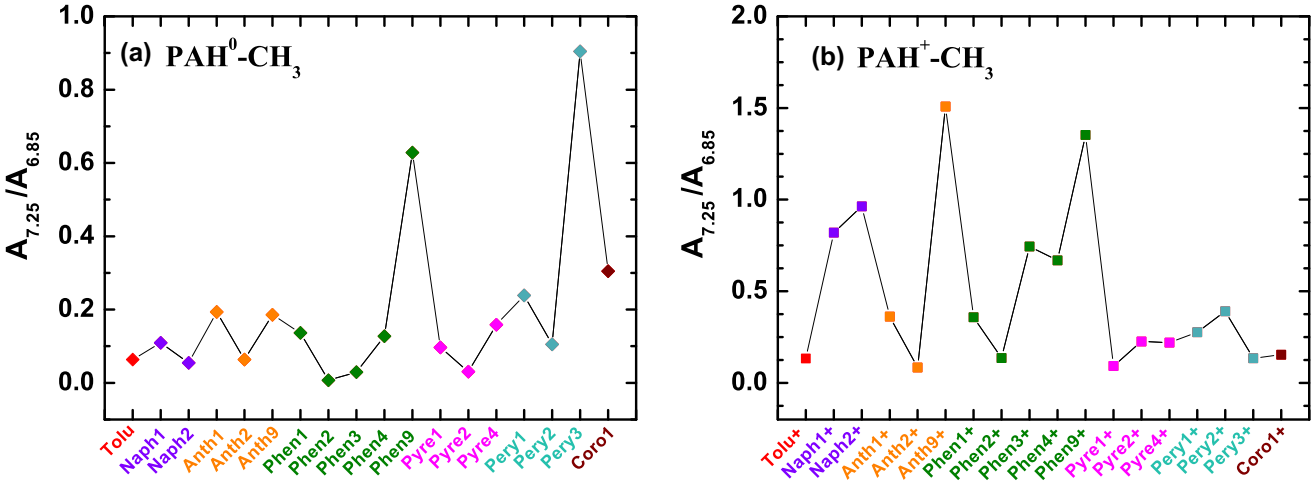

Figure 10. Comparison of the intrinsic strength of the 7.25 μm aliphatic C–H deformation with that of the 6.85 μm aliphatic C–H deformation for (a) neutral methyl PAHs and (b) ionized methyl PAHs.

6.85 μm aliphatic C–H deformation with the intrinsic band strengths of these two features computed from density functional theory for seven PAH molecules (and their cations) with a methyl side chain. We derive the fraction of C atoms in methyl(ene) aliphatic form to be at most ∼10 per cent, confirming the earlier finding that the UIE emitters are largely aromatic.

ACKNOWLEDGEMENTS

We thank T. Onaka, J.Y. Seok, G. Sloan, and the anonymous referee for very helpful suggestions. AL and XJY are supported in part by NSFC 11473023, NSF AST-1109039, NNX13AE63G, Hunan Provincial NSF 2015JJ3124, and the University of Missouri Research Board. RG is supported in part by NSF-PRISM grant Mathematics and Life Sciences (0928053). Acknowledgment is also made to the donors of the American Chemical Society Petroleum Research Fund for partial support of this research (53415-ND4). Computations were performed using the high-performance computer resources of the University of Missouri Bioinformatics Consortium.

REFERENCES

Acke B., Bouwman J., Juhász A., Henning T., van den Ancker M. E., Meeus G., Tielens A. G. G. M., Waters L. B. F. M., 2010, ApJ, 718, 558
Allamandola L. J., Tielens A. G. G. M., Barker J. R., 1985, ApJ, 290, L25
Allamandola L. J., Tielens A. G. G. M., Barker J. R., 1989, ApJS, 71, 733
Allamandola L. J., Hudgins D. M., Sandford S. A., 1999, ApJ, 511, L115
Barker J. R., Allamandola L. J., Tielens A. G. G. M., 1987, ApJ, 315, L61
Bernstein M. P., Sandford S. A., Allamandola L. J., 1996, ApJ, 472, L127
Borowski P., 2012, J. Phys. Chem. A, 116, 3866
Cramer C. J., 2004, Essentials of Computational Chemistry: Theories and Models, 2nd edn. John Wiley & Sons, New York
Chiar J. E., Tielens A. G. G. M., Whittet D. C. B., Schutte W. A., Boogert A. C. A., Lutz D., van Dishoeck E. F., Bernstein M. P., 2000, ApJ, 537, 749
Dartois E., Muñoz-Caro G. M., 2007, A&A, 476, 1235
Draine B. T., Li A., 2001, ApJ, 551, 807
Draine B. T., Li A., 2007, ApJ, 657, 810
Duley W. W., Williams D. A., 1981, MNRAS, 196, 269
d'Hendecourt L. B., Allamandola L. J., 1986, A&AS, 64, 453
Frisch M. J. et al., 2009, Gaussian 09, Revision B01. Gaussian, Inc., Wallingford, CT
Gillett F. C., Forrest W. J., Merrill K. M., 1973, ApJ, 183, 87
Hudgins D. M., Allamandola L. J., 2005, in Lis D. C., Blake G. A., Herbst E. eds, IAU Symp. 231, Astrochemistry: Recent Successes and Current Challenges. Cambridge Univ. Press, Cambridge, p. 443
Jones A. P., Duley W. W., Williams D. A., 1990, QJRAS, 31, 567
Kwok S., Zhang Y., 2011, Nature, 479, 80
Kwok S., Zhang Y., 2013, ApJ, 771, 5
Léger A., Puget J., 1984, A&A, 137, L5
Li A., 2004, in Witt A. N., Clayton G. C., Draine B. T., eds, ASP Conf. Ser. Vol. 309, Astrophysics of Dust. Astron. Soc. Pac., San Francisco, p. 417
Li A., 2005, in Popescu C. C., Tuffs R. J., eds, AIP Conf. Ser. Vol. 761, The Spectral Energy Distributions of Gas-rich Galaxies: Confronting Models with Data. Astron. Soc. Pac, San Francisco, p. 123
Li A., Draine B. T., 2001, ApJ, 554, 778
Li A., Draine B. T., 2012, ApJ, 760, L35
Mathis J. S., Mezger P. G., Panagia N., 1983, A&A, 128, 212 (MMP83)
Papoular R., Conrad J., Giuliano M., Kister J., Mille G., 1989, A&A, 217, 204
Peeters E., Hony S., Van Kerckhoven C., Tielens A. G. G. M., Allamandola L. J., Hudgins D. M., Bauschlicher C. W., 2002, A&A, 390, 1089
Pendleton Y. J., Allamandola L. J., 2002, ApJS, 138, 75
Riechers D. A. et al., 2014, ApJ, 796, 84
Rouillé G. et al., 2012, ApJ, 752, 25
Sakata A., Wada S., Onaka T., Tokunaga A. T., 1990, ApJS, 353, 543
Sandford S. A., Bernstein M. P., Materese C. K., 2013, ApJS, 205, 8
Seok J. Y., Li A., 2016, ApJ, in press
Sloan G. C. et al., 2005, ApJ, 632, 956
Sloan G. C. et al., 2014, ApJ, 791, 28
Steglich M., Jäger C., Huisken F., Friedrich M., Plass W., Räder H.-J., Müllen K., Henning Th., 2013, ApJS, 208, 26
Tielens A. G. G. M., 2008, ARA&A, 46, 289
Tokunaga A. T., 1997, in Okuda H., Matsumoto T., Roellig T., eds, ASP Conf. Ser. Vol. 124, Diffuse Infrared Radiation and the IRTS, Astron. Soc. Pac., San Francisco, p. 149
Yang X. J., Glaser R., Li A., Zhong J. X., 2013, ApJ, 776, 110
Yang X. J., Li A., Glaser R., Zhong J. X., 2016, ApJ, 825, 22
Zhang Y., Kwok S., Hrivnak B. J., 2010, ApJ, 725, 990

This paper has been typeset from a TEX/LATEX file prepared by the author.